Highly Selective and Efficient Perdeuteration of n-Pentane via H/D Exchange Catalyzed by a Silica-Supported Hafnium-Iridium Bimetallic Complex

Andrey V Pichugov, Léon Escomel, Sébastien Lassalle, Julien Petit, Ribal Jabbour, David Gajan, Laurent Veyre, Emiliano Fonda, Anne Lesage, Chloé Thieuleux, et al.

How to cite: Angew. Chem. Int. Ed. 2024, e202400992
doi.org/10.1002/anie.202400992

Heterogeneous Catalysis

Highly Selective and Efficient Perdeuteration of n-Pentane via H/D Exchange Catalyzed by a Silica-Supported Hafnium-Iridium Bimetallic Complex

*Andrey V. Pichugov, Léon Escomel, Sébastien Lassalle, Julien Petit, Ribal Jabbour, David Gajan, Laurent Veyre, Emiliano Fonda, Anne Lesage, Chloé Thieuleux, and Clément Camp**

Abstract: A Surface OrganoMetallic Chemistry (SOMC) approach is used to prepare a novel hafnium-iridium catalyst immobilized on silica, **HfIr/SiO$_2$**, featuring well-defined [≡SiOHf($CH_2{}^tBu$)$_2$(μ-H)$_3$IrCp*] surface sites. Unlike the monometallic analogous materials **Hf/SiO$_2$** and **Ir/SiO$_2$**, which promote *n*-pentane deuterogenolysis through C–C bond scission, we demonstrate that under the same experimental conditions (1 bar D_2, 250 °C, 3 h, 0.5 mol %), the heterobimetallic catalyst **HfIr/SiO$_2$** is highly efficient and selective for the perdeuteration of alkanes with D_2, exemplified on *n*-pentane, without substantial deuterogenolysis (<2 % at 95 % conversion). Furthermore this **HfIr/SiO$_2$** catalyst is robust and can be re-used several times without evidence of decomposition. This represents substantial advance in catalytic H/D isotope exchange (HIE) reactions of C(sp^3)–H bonds.

[*] A. V. Pichugov, L. Escomel, S. Lassalle, J. Petit, L. Veyre, C. Thieuleux, C. Camp
Laboratory of Catalysis, Polymerization, Processes and Materials, CP2 M UMR 5128
Université de Lyon, Institut de Chimie de Lyon, CNRS, Université Lyon 1, CPE Lyon
43 Bd du 11 Novembre 1918, F-69616 Villeurbanne, France
E-mail: clement.camp@univ-lyon1.fr

R. Jabbour, D. Gajan, A. Lesage
Centre de RMN à Hauts Champs de Lyon CRMN, UMR5082
Université de Lyon, CNRS, ENS Lyon
Université Claude Bernard Lyon 1, 69100 Villeurbanne, France

E. Fonda
Synchrotron SOLEIL
L'Orme des Merisiers, Saint Aubin BP-48, 91192 Gif sur Yvette, France

Introduction

Catalytic hydrogen isotope exchange (HIE) reactions are highly relevant to the industry for the late-stage incorporation of ^{2}H or ^{3}H into organic substrates.[1,2] This allows, among other things, the preparation of bioanalytical standards used for the understanding of toxicity and pharmacokinetic properties which are critical for most pharmaceutical and agrochemical companies.[3–6] HIE of C(sp^3)–H bonds is also relevant for the decontamination of tritium-containing radioactive waste oils from nuclear facilities,[7–11] or for the deuteration of organic materials,[12–14] for instance to increase the performances of OLEDs.[15–19] Besides, perdeuterated alkanes are useful as solvents and probes for NMR studies,[20] as analytical standards for improved GC/MS data analysis,[21] and have received attention to prevent counterfeiting, for example to identify illegal fuels.[22] Several homogeneous catalysts have been developed for H/D exchange reactions of C(sp^2)–H bonds,[1,2,23–27] with great success. However, the successful activation and labelling of C(sp^3)–H is much less established.[2,27] Furthermore, many of these molecular catalysts suffer from one or more severe limitations such as (i) the use of sophisticated ligands, (ii) the need to have orienting functional groups on the substrate, (iii) the use of hydrogen isotope sources less relevant than $^xH_2$ (x=2,3), (iv) thermal deactivation or (v) poor solvent compatibility (frequent use of chlorinated solvents that are poorly adapted for industrial applications). Heterogenized catalysts can overcome these issues and are thus valuable to improve HIE technologies, but to date homogeneous HIE catalysts development largely dominates the field.[2,27,28] Most known heterogeneous HIE catalysts contain poorly-defined active sites (typically noble metals on carbon),[28–35] so it is difficult to draw reliable structure–activity relationships for rational catalyst improvement. Perdeuteration of unactivated C–H bonds in alkanes thus remains a challenging goal: the development of effective technologies working in neat condition, scalable and compatible with continuous flow processes are therefore desirable.

The deuterium sources typically used for alkanes HIE are C_6D_6,[36] or *i*PrOD and D_2O under hydrothermal conditions.[11,30,37–39] Using gaseous D_2 or T_2 would be preferred due to their higher isotopic purity, but also for

atom economy reasons (C_6D_6 or D_2O are prepared from D_2) and the possibility to use a larger range of metal hydride catalysts, which are often not stable in the presence of water. Additionally, T_2 has a much lower radiotoxicity and higher stability than T_2O, which decomposes by autoradiolysis.[1,40] The major roadblock preventing the use of $^2H_2$ for alkane deuteration is the hydrogenolysis side-reaction, which emanates from C–C bond scission and results in a distribution of smaller alkanes. Alkane hydrogenolysis is commonplace and well documented for a range of early metal single sites[41–52] as well as late transition metal heterogeneous catalysts.[53–69] Competition between HIE and hydrogenolysis processes is far less scrutinized so far,[70] and selective catalysts able to label alkanes using D_2 or T_2 without promoting hydrogenolysis are lacking to our knowledge.

In continuation of our work on heterobimetallic catalysts,[71–76] we report a surface organometallic chemistry (SOMC) approach[77] to prepare a novel, well-defined, hafnium-iridium catalyst immobilized on silica. While SiO_2 supported monometallic hafnium and iridium catalysts promote *n*-pentane deuterogenolysis, under the same experimental conditions, the hafnium-iridium analogue is highly efficient and selective for the perdeuteration of alkanes with D_2, exemplified on *n*-pentane, without substantial deuterogenolysis.

Results and Discussion

Our group recently reported the preparation of an original hafnium-iridium polyalkyl polyhydride complex, noted **1** (Scheme 1).[78] We first considered the immobilization of **1** onto a SBA-15 silica support dehydroxylated at 700 °C ($SBA\text{-}15_{700}$), featuring a low density of surface hydroxyl groups (ca. 0.5 ≡Si–OH groups *per* nm^2), required for ensuring sites-isolation (route A in Scheme 1).[75,77] Upon treatment of $SBA\text{-}15_{700}$ with a pentane solution of **1** at r.t., the characteristic sharp IR band at 3748 cm^{-1} (Figure S8), corresponding to isolated surface silanols *ν*(OH), disappears while new signals attributed to metal-hydride stretches[73,79,80] at 1976 cm^{-1} and to *ν*(CH) stretches of the neopentyl and Cp* ligands at 2780–2990 cm^{-1} appear (Figure 1). 1 equiv. of neopentane is evolved *per* grafted Hf, as quantified by GC. These analyses are consistent with the covalent grafting of complex **1** onto silica via protonolysis of one Hf–Np group by a surface silanol, yielding a monopodal surface species, [≡SiOHf($CH_2{}^tBu$)$_2$(μ-H)$_3$IrCp*], **2-s**. The elemental analysis for **HfIr/SiO$_2$_A** (Expected: weight %C 11.57, %H 1.89, %Hf 8.60, %Ir 9.26 Found: %C 11.28, %H 1.88, %Hf 8.84, %Ir 9.60) is in excellent agreement with the proposed formula for **2-s**, and corresponds to 0.5 organometallic sites *per* nm^2 of silica, as expected.[75]

The reaction of **1** with 1 equiv. of *tris*(tert-butoxy)silanol was also investigated to provide a structural model of the silica-supported organometallic species **2-s**.[73,75,81,82] The protonolysis reactivity of **1** is well-behaved and yields the mono-substituted complex [Hf{OSi(O^{t}Bu)$_3$}($CH_2{}^tBu$)$_2$(μ-H)$_3$IrCp*], **2** as the sole reaction product detected upon ^{1}H NMR reaction monitoring. Complex **2** was fully characterized by elemental analysis, X-ray crystallography (structure displayed on Figure 2), NMR (Figures S1 to S3) and IR spectroscopies (Figure S7). The spectroscopic and structural features of **2** are for most part unaffected by the substitution of one neopentyl ligand by one siloxide and match the spectroscopic data for the surface species **2-s**. In particular, the Hf–Ir distance in **2** (2.6981(8) Å) is similar to that in **1** (2.6773(4) Å),[78] and the metal-hydride stretching signal in the DRIFT spectrum for **2** (1987 cm^{-1}) is in the same range as that for **1** and **2-s** (1982 cm^{-1} and 1975 cm^{-1}, respectively).

From these experiments we conclude that (i) the reactivity of **1** towards Si–OH groups is selective and leads to monopodal Hf-siloxy species; (ii) the coordination sphere and geometry of the two metal centers is for most part unaffected by this ligand substitution.

Two-dimensional (2D) proton double- (DQ) and triple-quantum (TQ) NMR experiments were applied to confirm

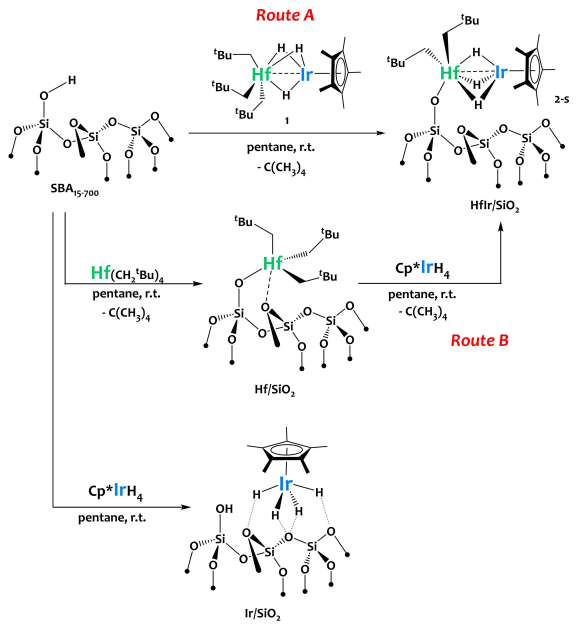

Scheme 1. Preparation of the silica-supported monometallic and heterobimetallic catalysts.

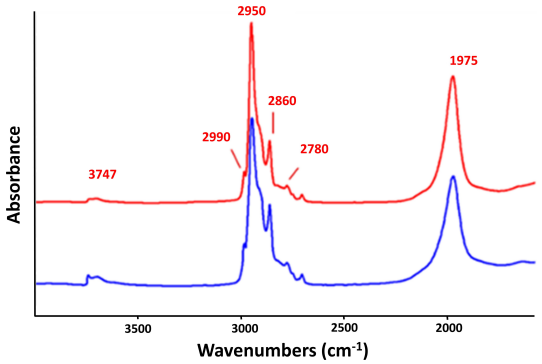

Figure 1. Diffuse reflection infrared Fourier transform spectra of material **HfIr/SiO$_2$** prepared via route A (red line) and route B (blue line).

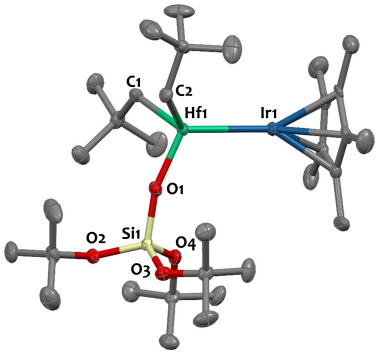

Figure 2. Solid-state molecular structure of **2** (30% probability ellipsoids).[83] Hydrogen atoms have been omitted for clarity. Selected bond lengths (Å) and angles (°): Hf1–Ir1 2.6981(8), Hf1–O1 1.916(7), Hf1–C1 2.20(1), Hf1–C2 2.21(1), Ir1–Cp*centroid 1.843(5), Hf1–Ir1–Cp*centroid 179.2(3), Si1–O1–Hf1 156.1(5).

the tris-hydride nature of the surface species **2-s** in **HfIr/SiO$_2$_A**. This spectroscopic method has been previously applied in our group to successfully distinguish monohydride, bishydride and trishydride surface species.[73,75] Here, well-defined autocorrelations are observed for the hydride resonance in both the DQ and TQ correlation spectra (Figure 3 and S6). In particular, the correlation along the $\omega_1 = 3\omega_2$ line is a clear indication for the presence of a set of three dipolar-coupled protons. The TQ-SQ correlation spectrum shows also the expected autocorrelations for the CH_3 groups of the Cp* and ^{t}Bu moieties, as well as the expected off-diagonal correlation with the hydrides in agreement with the proposed structure for **2-s**.

Extended X-ray absorption fine structure (EXAFS) experiments at the Hf L_{III} edge of **HfIr/SiO$_2$_A** were performed to confirm the local structure of the surface species. The best fit (Table S2, reduced $\chi^2 = 1.5$) gives a first shell of one oxygen atom at 1.94(1) Å, one iridium atom at 2.68(1) Å and two carbons at 2.10(1) and 2.24(1) Å. All these distances are in excellent agreement with the metrical parameters determined by X-ray crystallography on the molecular model **2** (Figure 2).

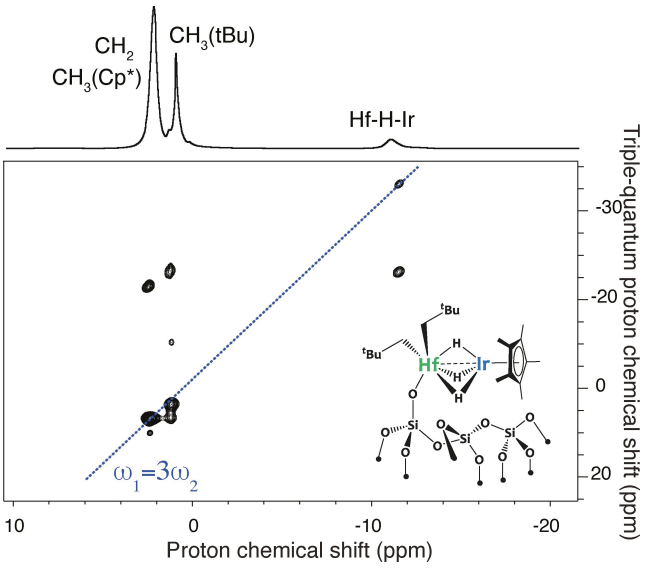

Figure 3. Proton SQ-TQ NMR spectrum of **2-s**. The trace above the 2D plot corresponds to the one-dimensional ^{1}H NMR spectrum. The dotted blue line corresponds to the $\omega_1 = 3\omega_2$ diagonal. The autocorrelation peak at around (−11.5 ppm, −34.5 ppm) is clearly observed.

The monometallic monopodal silica surface organometallic complex [≡SiOHf($CH_2{}^tBu$)$_3$] was obtained upon grafting Hf($CH_2{}^tBu$)$_4$ onto SBA-15$_{700}$ at room temperature (Scheme 1), as reported previously.[84] The resulting material, **Hf/SiO$_2$**, was then treated with a pentane solution of Cp*IrH$_4$ at room temperature, using a Hf:Ir stoichiometric ratio of 1:1, yielding a white material, noted **HfIr/SiO$_2$_B**. 0.9 equiv. of neopentane is released *per* surface Hf atom, as titrated by gas chromatography. This analysis is consistent with the protonolysis reaction of one neopentyl group from the hafnium surface species, [≡SiOHf($CH_2{}^tBu$)$_3$], with Cp*IrH$_4$, yielding complex **2-s**. This is further supported by the IR spectroscopy analysis of **HfIr/SiO$_2$_B** which is identical to that of **HfIr/SiO$_2$_A** (Figure 1). The ^{1}H and ^{13}C solid-state NMR spectra of **HfIr/SiO$_2$_A** and **HfIr/SiO$_2$_B** are identical and exhibit the expected signals for the Cp*, Np and hydride ligands (Figure S4), in agreement with the proposed structure. The similarity of the IR and NMR signatures of **HfIr/SiO$_2$_A** and **HfIr/SiO$_2$_B** indicates that the same surface species, **2-s**, is obtained using both routes (A and B), suggesting the equivalence of these synthetic approaches. This contrasts with our previous work with a tantalum/iridium system, where strong disparities between both routes were noticed due to the formation of trinuclear species in route B,[73] as a result of polyaddition of Cp*IrH$_4$ which seems precluded in the case of hafnium. Note that neither **1** nor **2** further react with Cp*IrH$_4$, which also explains why the dinuclear species **2-s** is selectively formed in the present case. For sake of comparison, we also prepared a monometallic **Ir/SiO$_2$** benchmark, through physisorption of Cp*IrH$_4$ at the surface of SBA-15$_{700}$, as described previously[72] (Scheme 1).

We then proceeded to evaluation of the catalytic potential of this new heterobimetallic species towards C-(sp^3)–H/D exchange. The test reaction between *n*-C_5H_{12} (40 mbar, 1 mmol, 1 equiv.) and D_2 (1000 mbar, 25 mmol, 25 equiv.) at 0.5 mol% of catalyst loading (with respect to C_5H_{12}) was used to compare the performances of **HfIr/SiO$_2$_A** with aforementioned monometallic analogs **Hf/SiO$_2$** and **Ir/SiO$_2$**.

In the first series of experiments, the reactor containing the catalyst portion (as powder) and both reagents in the gas phase was heated to 250 °C. Under these experimental conditions, two types of transformations can occur concomitantly: i) hydrogen/deuterium exchange of *n*-pentane producing deuteropentanes - named D_x–C_5 thereafter and ii) C–C deuterogenolysis of *n*-pentane and/or deuteropentanes forming mixture of lighter deuterated alkanes, named C_1–C_4 thereafter (see Scheme 2). To get insights into the selectivity of the process, we quantified the contribution of reactions (i) and (ii) upon regularly monitoring the gas phase by GC-MS and GC-FID.

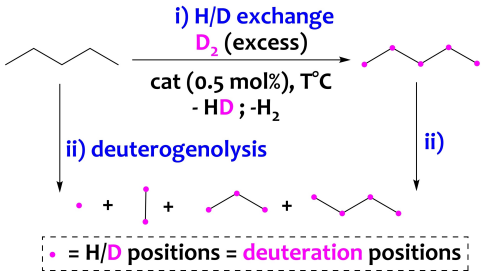

Scheme 2. Two possible pathways in the reaction of *n*-pentane with D_2 in the presence of the catalysts (0.5 mol%) upon heating: i) H/D exchange of *n*-pentane yielding deuteropentanes. ii) C–C deuterogenolysis of *n*-C_5H_{12} and/or deuteropentanes producing lighter (deutero)alkanes (from C_1 to C_4).

The obtained kinetic data are summarized in Figure 4. The first striking observation is the high HIE activity of the heterobimetallic catalyst **HfIr/SiO$_2$_A**: the proportion of D_x–C_5 quickly increases until reaching a value higher than 90% after 3h while C_5H_{12} is rapidly consumed (Figure 4a). Importantly, almost no deuterogenolysis activity is noticed: less than 2% of lighter alkanes (from C_1 to C_4) is observed in the reaction medium after 3 hours of reaction. Therefore, **HfIr/SiO$_2$_A** features a very high selectivity (>99%) for the H/D exchange of pentane at high conversion of pentane (95%, see Figure S15). Note that material **HfIr/SiO$_2$_B** exhibits the same catalytic performance as **HfIr/SiO$_2$_A** in these conditions (Figure S13), confirming that both materials contain the same surface sites, as suggested by the spectroscopic characterizations.

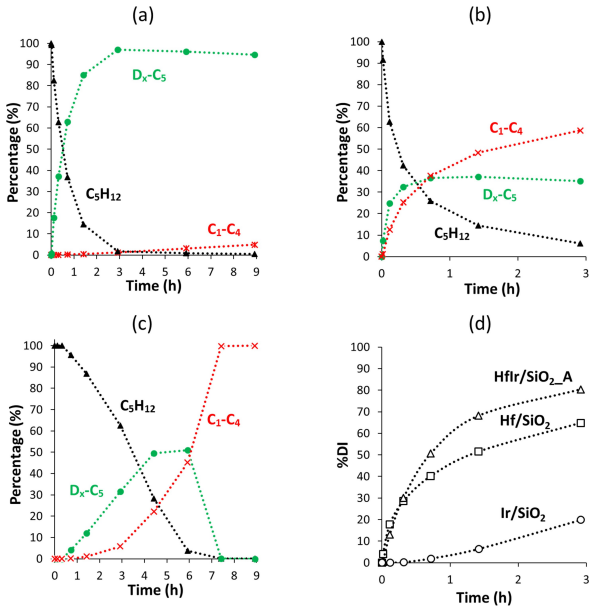

Figure 4. Catalytic performance of **HfIr/SiO$_2$_A** (a), **Hf/SiO$_2$** (b) and **Ir/SiO$_2$** (c) in deuterogenolysis and HIE of *n*-pentane (C_5H_{12}) at **250 °C**, giving lighter (deutero)alkanes (C_1–C_4) and deuteropentanes (D_x–C_5), respectively. (d) Evolution of deuterium incorporation in *n*-pentane (% DI) during the reaction.

In contrast, the monometallic catalyst **Hf/SiO$_2$** exhibits a moderate pentane HIE activity: the D_x–C_5 amount increases very progressively (40% after 3 hours of reaction, see Figure 4b). Moreover, an important C–C deuterogenolysis activity is noticed at the beginning of the reaction (about 40% of lighter alkanes is present in the reaction mixture after 60 minutes). This deuterogenolysis activity then gradually drops with time suggesting the rapid deactivation of the catalyst under these experimental conditions. Note that the incorporation of hafnium in the silica matrix, via the formation of inert $[(\equiv SiO)_4Hf]$, $[(\equiv SiO)_2SiH_2]$ and $[(\equiv SiO)_3SiH]$ surface sites, was previously reported.[85] Similarly, catalyst **Ir/SiO$_2$** displays poor activity and selectivity towards HIE of *n*-pentane at 250 °C (Figure 4c). The proportion of deuteropentanes (D_x–C_5) slowly increases up to 50% within 4 hours and quickly falls after due to prevailing deuterogenolysis process and complete transformation of all C_5 components into shorter alkanes. Analysis of the deuterium incorporation in pentane (%DI) in the course of reaction confirms the high HIE activity of **HfIr/SiO$_2$_A** system (the maximum equilibrium value, $\%DI_{eq} \approx 80\%$, is quickly reached within 60 minutes) in comparison with both monometallic precursors (Figure 4d).

STEM analysis of the spent catalysts revealed the presence of small Ir Nps with a mean size of 1.8 ± 0.3 nm at the surface of the SBA-15_{700} support for catalyst **Ir/SiO$_2$** (Figure 5a). The gradual formation of these Nps in presence of D_2 is likely responsible for the observed inductive increase in deuterogenolysis rate. In contrast, no particles with a mean diameter exceeding 1 nm were discernible on the images of the spent **HfIr/SiO$_2$** catalyst after reaction at 250 °C (Figure 5b), although the surface roughness observed in the images may imply the generation of small clusters. Importantly, the heterobimetallic catalyst **HfIr/SiO$_2$** showed some robustness since three catalytic runs were performed consecutively with identical activity and selectivity (for each cycle the gas phase was evacuated, fresh portions of *n*-pentane and D_2 were loaded into the reactor, then the reaction was run under the same experimental conditions—see Figure S10). Therefore, whatever the exact nature of the active sites in **HfIr/SiO$_2$**, we can confidently conclude that these are not nanoparticles and are rather robust in these experimental conditions.

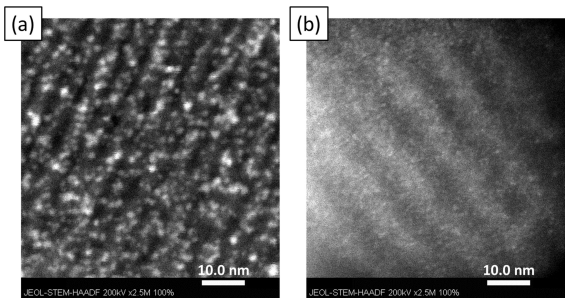

Figure 5. STEM-HAADF micrographs of spent catalysts after reaction at 250 °C: **Ir/SiO$_2$** (a), **HfIr/SiO$_2$** (b).

Remarkably, upon initial pretreatment of catalyst **HfIr/SiO$_2$_A** at 500 °C in a D_2 atmosphere (1 bar, 15 hours), subsequent utilization in catalysis at 250 °C under the same experimental conditions results in a reversed activity pattern. This reversed pattern mirrors that observed for **Ir/SiO$_2$**, with significant deutrogenolysis, as illustrated in Figure 6. Analysis of the spent heterobimetallic catalyst by STEM shows the clear formation of nanoparticles. This implies that the heterobimetallic catalyst is unstable at 500 °C, and that the presence of Nps seems to play a key role in promoting C–C bond cleavage.

A catalytic test was also conducted using molecular complex **1** as a benchmark. The complex was dissolved in pentane, added to the reactor, and the solvent was evaporated. The gas phase (pentane + D_2) was then introduced, and the reactor was heated to 250°C. This resulted in a noticeable change in the catalyst's appearance, from a white solid powder to a black oily substance. The catalytic results showed a significant deuterogenolysis activity (Figure S16), likely due to the degradation of the complex into metal nanoparticles.

In order to try to prevent both deuterogenolysis and catalyst decomposition, the catalytic activity of all materials was then studied at lower temperature (125 °C). Under these conditions, the monometallic **Ir/SiO$_2$** catalyst turned out to be inactive (Figure 7c). Such decrease in temperature allowed improving significantly the performance of **Hf/SiO$_2$**, which features a faster deuterium incorporation rate than that for **HfIr/SiO$_2$** at 125 °C (Figure 7d). However, the monometallic catalyst, **Hf/SiO$_2$**, is still poorly selective under these conditions: >50 % deuterogenolysis occurred when maximum deuteration of pentane is reached after 6 h (Figure 7b). Although slower, the heterobimetallic catalyst **HfIr/SiO$_2$** can, in contrast, reach equilibrium (ca. 80 % DI) after 24 hours at 125 °C with 100 % selectivity (no deuterogenolysis, see Figure 7a).

It is important to note that the examination of the spent catalysts through STEM reveals distinct formation of inactive Ir nanoparticles at 125 °C for **Ir/SiO$_2$** (Figure 8a). In contrast, STEM images recorded for the spent **HfIr/SiO$_2$** catalyst (Figure 8b) clearly indicate the absence of such nanoparticles, in favor of molecular active sites. Post-catalysis DRIFTS experiments recorded on the spent **HfIr/SiO$_2$** catalyst (Figure S9) clearly show a decrease in intensity of $\nu(C_{sp3}–H)$ bands and the unequivocal emergence of new $\nu(C_{sp3}–D)$, aligning with expectations regarding the deuteration of alkyl ligands within the surface species. Furthermore, the characteristic ν(Ir–H) vibration displays a decrease in intensity, indicative of deuteration of the bridging hydrides in the surface species, without significant alterations in shape or energy. These observations suggest that the structural integrity of the active species remains intact during catalysis. While the appearance of ν(Ir–D) vibrations is anticipated, unfortunately, their detection experimentally is impeded by overlap with the strong signal contribution from the ν(Si–O) bands originating from the silica support.

In these systems, pentane deuteration most likely occurs through sigma-bond metathesis[86,87] (Scheme S1-a) and/or heterolytic C–H bond activation across the two metals[74,76]

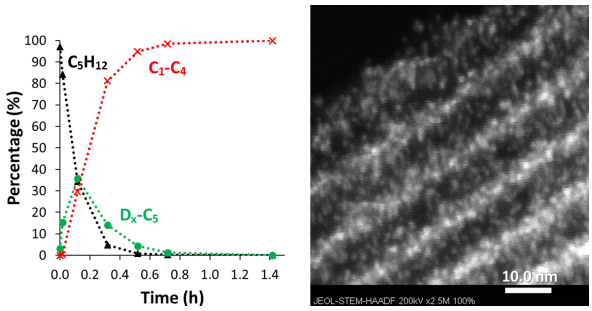

Figure 6. Left: catalytic performance of **HfIr/SiO$_2$_A** which was pre-treated at 500 °C, in deuterogenolysis and HIE of *n*-pentane (C_5H_{12}) at 250 °C. Right: STEM-HAADF micrograph of **HfIr/SiO$_2$_A** after treatment with D_2 (500 °C, 15 hours) confirming formation of small Nps.

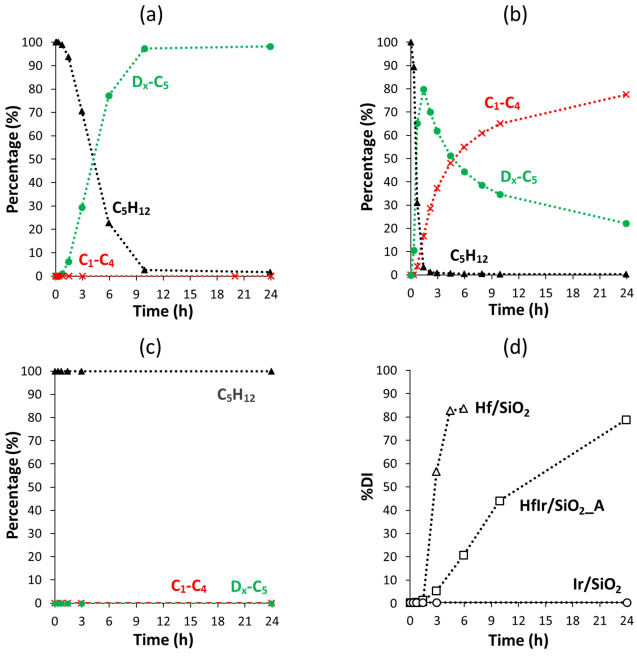

Figure 7. Catalytic performance of **HfIr/SiO$_2$_A** (a), **Hf/SiO$_2$** (b) and **Ir/SiO$_2$** (c) in deuterogenolysis and HIE of *n*-pentane (C_5H_{12}) at **125 °C**, giving lighter (deutero)alkanes (C_1–C_4) and deuteropentanes (D_x–C_5), respectively. (d) Evolution of deuterium incorporation in *n*-pentane (% DI) during the reaction.

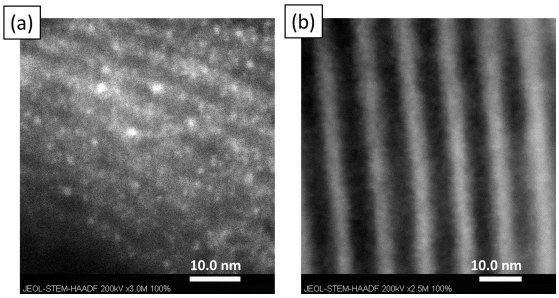

Figure 8. STEM-HAADF micrographs of spent catalysts after 125 °C: **Ir/SiO$_2$** (a), **HfIr/SiO$_2$** (b).

(Scheme S1-b). Cleavage of carbon–carbon bonds in the skeleton of alkanes by d^0 group IV metal catalysts is known to occur through β-alkyl transfer (Scheme S2-a).[88,89] This elementary step is favored in environments with highly electron-deficient group IV metal sites, marked by low electron counts and minimal steric hindrance. Within the HfIr system described here, the presence of the iridium center and the bridging hydrides may mitigate the electron deficiency of the Hf(IV) sites, consequently diminishing the likelihood of this pathway. Alkane hydrogenolysis activity and selectivity is also known to be sensitive on the structure and nanoparticle size of Ir catalysts.[90–92] Indeed, studies have shown that as particle size decreases below an optimal diameter (ca. 1.4 nm), alkane hydrogenolysis activity can decrease significantly.[90] Such structure sensitivity suggests that the cleavage of C–C bond in alkanes proceeds through intermediates bound to the surface via multiple metal atoms on clusters or nanoparticles (Scheme S2-b).[93] While the minimum ensemble size required for alkane hydrogenolysis remains uncertain, smaller Ir_4 clusters have been found to exhibit lower hydrogenolysis activity compared to larger Ir aggregates, as observed in propane hydrogenolysis.[94] Our findings are consistent with these earlier observations, indicating that Ir nanoparticles promote deuterogenolysis, while the well-defined dual-atom molecular species **2-s** does not.

Conclusion

In summary, a SOMC approach was used to prepare a well-defined heterobimetallic catalyst, **HfIr/SiO$_2$**, which is highly efficient for the perdeuteration of alkanes, illustrated here on *n*-pentane. Importantly, this **HfIr/SiO$_2$** catalyst shows improved stability and selectivity in thermal conditions compared to monometallic analogues **Hf/SiO$_2$** and **Ir/SiO$_2$**. This represents substantial advance in catalytic H/D isotope exchange reactions of C(sp^3)–H bonds.

Supporting Information

The authors have cited additional references within the Supporting Information.[72,78,84,95–113]

Acknowledgements

Co-funded by the French National Research Agency (ANR) (grant number ANR-21-CE07-0009-01, SHICC) and the European Union (ERC, DUO, 101041762). Views and opinions expressed are however those of the authors only and do not necessarily reflect those of the European Union or the European Research Council. Neither the European Union nor the granting authority can be held responsible for them. We acknowledge SOLEIL for provision of synchrotron radiation facilities (SAMBA beamline, proposal 20181971) and Infranalytics CNRS FR-2054 for access to high-field NMR equipment. We thank Erwann Jeanneau from the Centre de Diffractométrie Henri Longchambon for help with the XRD analysis.

Conflict of Interest

The authors declare no conflict of interest.

Data Availability Statement

XRD data openly available from the joint Cambridge Crystallographic Data Centre and Fachinformationszentrum Karlsruhe Access Structures service. Experimental details, NMR and IR spectra, XRD and EXAFS data, catalysis kinetic data, STEM-HAADF images in article supplementary material. Other data available open reasonable request from the authors.

[1] R. Pony Yu, D. Hesk, N. Rivera, I. I. Pelczer, P. J. Chirik, *Nature* **2016**, *529*, 195–199.
[2] J. Atzrodt, V. Derdau, W. J. Kerr, M. Reid, *Angew. Chem. Int. Ed.* **2018**, *57*, 3022–3047.
[3] W. J. S. Lockley, A. McEwen, R. Cooke, *J. Labelled Compd. Radiopharm.* **2012**, *55*, 235–257.
[4] E. M. Isin, C. S. Elmore, G. N. Nilsson, R. A. Thompson, L. Weidolf, *Chem. Res. Toxicol.* **2012**, *25*, 532–542.
[5] D. Hesk, C. F. Lavey, P. McNamara, *J. Labelled Compd. Radiopharm.* **2010**, *53*, 722–730.
[6] J. Atzrodt, V. Derdau, W. J. Kerr, M. Reid, *Angew. Chem. Int. Ed.* **2018**, *57*, 1758–1784.
[7] T. Takeishi, K. Kotoh, Y. Kawabata, J. I. Tanaka, S. Kawamura, M. Iwata, *Fusion Sci. Technol.* **2015**, *67*, 596–599.
[8] A. B. Sazonov, É. P. Magomedbekov, G. V. Veretennikova, S. A. Samoilov, A. V. Zharkov, *At. Energy* **2005**, *98*, 127–134.
[9] É. P. Magomedbekov, V. A. Shalygin, O. A. Baranova, M. Y. Isaeva, A. V. Zharkov, *At. Energy* **2005**, *98*, 122–126.
[10] L. Dong, N. Yang, Y. Yang, W. Li, Y. Quan, B. Deng, D. Meng, Y. Du, S. Li, Z. Tan, *RSC Adv.* **2017**, *7*, 890–896.
[11] J. R. Jones, P. B. Langham, S. Y. Lu, *Green Chem.* **2002**, *4*, 464–466.
[12] L. Li, J. Jakowski, C. Do, K. Hong, *Macromolecules* **2021**, *54*, 3555–3584.
[13] M. Zak, J. Herman, M. Czerwiński, Y. Arakawa, H. Tsuji, P. Kula, *Liq. Cryst.* **2023**, *50*, 622–635.
[14] M. Pytlarczyk, J. Herman, Y. Arakawa, H. Tsuji, P. Kula, *J. Mol. Liq.* **2022**, *345*, 117847.
[15] C. T. Chun, C. H. Kuo, *J. Phys. Chem. C* **2007**, *111*, 3490–3494.
[16] H. Tsuji, C. Mitsui, E. Nakamura, *Chem. Commun.* **2014**, *50*, 14870–14872.
[17] S. Jung, W. L. Cheung, S. jie Li, M. Wang, W. Li, C. Wang, X. Song, G. Wei, Q. Song, S. S. Chen, W. Cai, M. Ng, W. K. Tang, M. C. Tang, *Nat. Commun.* **2023**, *14*, 1–12.

[18] J. Yao, S. C. Dong, B. S. T. Tam, C. W. Tang, *ACS Appl. Mater. Interfaces* **2023**, *15*, 7255–7262.
[19] H. J. Bae, J. S. Kim, A. Yakubovich, J. Jeong, S. Park, J. Chwae, S. Ishibe, Y. Jung, V. K. Rai, W. J. Son, S. Kim, H. Choi, M. H. Baik, *Adv. Opt. Mater.* **2021**, *9*, 2100630.
[20] A. P. Ramos, M. Doroudgar, M. Lafleur, *Biochim. Biophys. Acta Biomembr.* **2020**, *1862*, 183201.
[21] E. Massold, *J. Chromatogr. A* **2007**, *1154*, 342–352.
[22] Y. Suzuki, T. Korenaga, Y. Chikaraishi, *Chem. Lett.* **2006**, *35*, 532–533.
[23] H. Yang, C. Zarate, W. N. Palmer, N. Rivera, D. Hesk, P. J. Chirik, *ACS Catal.* **2018**, *8*, 10210–10218.
[24] M. Daniel-Bertrand, S. Garcia-Argote, A. Palazzolo, I. Mustieles Marin, P. F. Fazzini, S. Tricard, B. Chaudret, V. Derdau, S. Feuillastre, G. Pieters, *Angew. Chem. Int. Ed.* **2020**, *59*, 21114–21120.
[25] W. J. Kerr, D. M. Lindsay, P. K. Owens, M. Reid, T. Tuttle, S. Campos, *ACS Catal.* **2017**, *7*, 7182–7186.
[26] W. J. Kerr, R. J. Mudd, M. Reid, J. Atzrodt, V. Derdau, *ACS Catal.* **2018**, *8*, 10895–10900.
[27] S. Kopf, F. Bourriquen, W. Li, H. Neumann, K. Junge, M. Beller, *Chem. Rev.* **2022**, *122*, 6634–6718.
[28] A. Palazzolo, T. Naret, M. Daniel-Bertrand, D. A. Buisson, S. Tricard, P. Lesot, Y. Coppel, B. Chaudret, S. Feuillastre, G. Pieters, *Angew. Chem. Int. Ed.* **2020**, *59*, 20879–20884.
[29] T. Kurita, K. Hattori, S. Seki, T. Mizumoto, F. Aoki, Y. Yamada, K. Ikawa, T. Maegawa, Y. Monguchi, H. Sajiki, *Chem. A Eur. J.* **2008**, *14*, 664–673.
[30] T. Maegawa, Y. Fujiwara, Y. Inagaki, H. Esaki, Y. Monguchi, H. Sajiki, *Angew. Chem. Int. Ed.* **2008**, *47*, 5394–5397.
[31] Y. Fujiwara, H. Iwata, Y. Sawama, Y. Monguchi, H. Sajiki, *Chem. Commun.* **2010**, *46*, 4977–4979.
[32] T. Maegawa, Y. Fujiwara, Y. Inagaki, Y. Monguchi, H. Sajiki, *Adv. Synth. Catal.* **2008**, *350*, 2215–2218.
[33] Y. Sawama, Y. Yabe, H. Iwata, Y. Fujiwara, Y. Monguchi, H. Sajiki, *Chem. A Eur. J.* **2012**, *18*, 16436–16442.
[34] H. Esaki, R. Ohtaki, T. Maegawa, Y. Monguchi, H. Sajiki, *J. Org. Chem.* **2007**, *72*, 2143–2150.
[35] J. Atzrodt, V. Derdau, *J. Labelled Compd. Radiopharm.* **2010**, *53*, 674–685.
[36] M. H. G. Prechtl, M. Teltewskoi, A. Dimitrov, E. Kemnitz, T. Braun, *Chem. A Eur. J.* **2011**, *17*, 14385–14388.
[37] S. Matsubara, Y. Yokota, K. Oshima, *Chem. Lett.* **2004**, *33*, 294–295.
[38] T. Yamada, Y. Sawama, K. Shibata, K. Morita, Y. Monguchi, H. Sajiki, *RSC Adv.* **2015**, *5*, 13727–13732.
[39] H. Sajiki, F. Aoki, H. Esaki, T. Maegawa, K. Hirota, *Org. Lett.* **2004**, *6*, 1485–1487.
[40] P. Morawietz, R. Weck, A. A. Scholte, J. Atzrodt, S. Güssregen, V. Derdau, *Green Chem.* **2022**, *24*, 5–11.
[41] L. d'Ornelas, S. Reyes, F. Quignard, A. Choplin, J.-M. Basset, *Chem. Lett.* **1993**, *22*, 1931–1934.
[42] J. Corker, F. Lefebvre, C. Lécuyer, V. Dufaud, F. Quignard, A. Choplin, J. Evans, J. M. Basset, *Science* **1996**, *271*, 966–969.
[43] K. K. Samudrala, M. P. Conley, *J. Am. Chem. Soc.* **2023**, *22*, 43.
[44] A. Q. Kane, A. M. Esper, K. Searles, C. Ehm, A. S. Veige, *Catal. Sci. Technol.* **2021**, *11*, 6155–6162.
[45] C. Lecuyer, F. Quignard, A. Choplin, D. Olivier, J.-M. Basset, *Angew. Chem. Int. Ed.* **1991**, *30*, 1660–1661.
[46] M. Chabanas, V. Vidal, C. Copéret, J. Thivolle-Cazat, J. M. Basset, *Angew. Chem. Int. Ed.* **2000**, *39*, 1962–1965.
[47] V. Polshettiwar, F. A. Pasha, A. De Mallmann, S. Norsic, J. Thivolle-Cazat, J. M. Basset, *ChemCatChem* **2012**, *4*, 363–369.
[48] F. Rataboul, M. Chabanas, A. De Mallmann, C. Copéret, J. Thivolle-Cazat, J. M. Basset, *Chem. A Eur. J.* **2003**, *9*, 1426–1434.
[49] Q. Lai, A. H. Mason, A. Agarwal, W. C. Edenfield, X. Zhang, T. Kobayashi, Y. Kratish, T. J. Marks, *Angew. Chem. Int. Ed.* **2023**, *62*, e202312546.
[50] A. H. Mason, A. Motta, A. Das, Q. Ma, M. J. Bedzyk, Y. Kratish, T. J. Marks, *Nat. Commun.* **2022**, *13*, 1–12.
[51] J. Gao, L. Zhu, M. P. Conley, *ACS Catal.* **2023**, *13*, 10765–10769.
[52] J. Gao, L. Zhu, M. P. Conley, *J. Am. Chem. Soc.* **2023**, *145*, 4964–4968.
[53] H. C. Yao, M. Shelef, *J. Catal.* **1979**, *56*, 12–20.
[54] J. R. Engstrom, D. W. Goodman, W. H. Weinberg, *J. Am. Chem. Soc.* **1988**, *110*, 8305–8319.
[55] A. Tennakoon, X. Wu, M. Meirow, D. Howell, J. Willmon, J. Yu, J. V. Lamb, M. Delferro, E. Luijten, W. Huang, A. D. Sadow, *J. Am. Chem. Soc.* **2023**, *145*, 17936–17944.
[56] X. Wu, A. Tennakoon, R. Yappert, M. Esveld, M. S. Ferrandon, R. A. Hackler, A. M. Lapointe, A. Heyden, M. Delferro, B. Peters, A. D. Sadow, W. Huang, *J. Am. Chem. Soc.* **2022**, *144*, 5323–5334.
[57] S. S. Borkar, R. Helmer, S. Panicker, M. Shetty, *ACS Sustainable Chem. Eng.* **2023**, *11*, 10142–10157.
[58] D. P. Estes, G. Siddiqi, F. Allouche, K. V. Kovtunov, O. V. Safonova, A. L. Trigub, I. V. Koptyug, C. Copéret, *J. Am. Chem. Soc.* **2016**, *138*, 14987–14997.
[59] J. Z. Tan, C. W. Hullfish, Y. Zheng, B. E. Koel, M. L. Sarazen, *Appl. Catal. B* **2023**, *338*, 123028.
[60] S. P. Ertem, C. E. Onuoha, H. Wang, M. A. Hillmyer, T. M. Reineke, T. P. Lodge, F. S. Bates, *Macromolecules* **2020**, *53*, 6043–6055.
[61] C. Wang, T. Xie, P. A. Kots, B. C. Vance, K. Yu, P. Kumar, J. Fu, S. Liu, G. Tsilomelekis, E. A. Stach, W. Zheng, D. G. Vlachos, *JACS Au* **2021**, *1*, 1422–1434.
[62] J. R. Engstrom, D. W. Goodman, W. H. Weinberg, *J. Am. Chem. Soc.* **1986**, *108*, 4653–4655.
[63] G. C. Bond, J. J. Garcia, *Catal. Sci. Technol.* **2017**, *7*, 5294–5300.
[64] D. Kalakkad, S. L. Anderson, A. D. Logan, J. Peña, E. J. Braunschweig, C. H. F. Peden, A. K. Datye, *J. Phys. Chem.* **1993**, *97*, 1437–1444.
[65] G. C. Bond, X. Yide, *J. Chem. Soc. Faraday Trans. 1* **1984**, *80*, 969–980.
[66] G. C. Bond, J. C. Slaa, *J. Mol. Catal. A* **1995**, *96*, 163–173.
[67] R. A. Hackler, J. V. Lamb, I. L. Peczak, R. M. Kennedy, U. Kanbur, A. M. Lapointe, K. R. Poeppelmeier, A. D. Sadow, M. Delferro, *Macromolecules* **2022**, *55*, 6801–6810.
[68] J. E. Rorrer, G. T. Beckham, Y. Román-Leshkov, *JACS Au* **2021**, *1*, 8–12.
[69] B. Du, X. Chen, Y. Ling, T. Niu, W. Guan, J. Meng, H. Hu, C. W. Tsang, C. Liang, *ChemSusChem* **2023**, *16*, e202202035.
[70] A. Sattler, *ACS Catal.* **2018**, *8*, 2296–2312.
[71] R. Srivastava, R. Moneuse, J. Petit, P.-A. A. Pavard, V. Dardun, M. Rivat, P. Schiltz, M. Solari, E. Jeanneau, L. Veyre, C. Thieuleux, E. A. Quadrelli, C. Camp, *Chem. A Eur. J.* **2018**, *24*, 4361–4370.
[72] L. Escomel, D. Abbott, V. Mougel, L. Veyre, C. Thieuleux, C. Camp, *Chem. Commun.* **2022**, *58*, 8214–8217.
[73] S. Lassalle, R. Jabbour, I. Del Rosal, L. Maron, E. Fonda, L. Veyre, D. Gajan, A. Lesage, C. Thieuleux, C. Camp, *J. Catal.* **2020**, *392*, 287–301.
[74] I. Del Rosal, S. Lassalle, C. Dinoi, C. Thieuleux, L. Maron, C. Camp, *Dalton Trans.* **2021**, *50*, 504–510.
[75] S. Lassalle, R. Jabbour, P. Schiltz, P. Berruyer, T. K. Todorova, L. Veyre, D. Gajan, A. Lesage, C. Thieuleux, C. Camp, *J. Am. Chem. Soc.* **2019**, *141*, 19321–19335.
[76] A. Lachguar, A. V. Pichugov, T. Neumann, Z. Dubrawski, C. Camp, *Dalton Trans.* **2023**, *53*, 1393–1409.

[77] C. Copéret, A. Comas-Vives, M. P. Conley, D. P. Estes, A. Fedorov, V. Mougel, H. Nagae, F. Núñez-Zarur, P. A. Zhizhko, *Chem. Rev.* **2016**, *116*, 323–421.
[78] S. Lassalle, J. Petit, R. L. Falconer, V. Hérault, E. Jeanneau, C. Thieuleux, C. Camp, *Organometallics* **2022**, *41*, 1675–1687.
[79] L. Escomel, N. Soulé, E. Robin, I. Del Rosal, L. Maron, E. Jeanneau, C. Thieuleux, C. Camp, *Inorg. Chem.* **2022**, *61*, 5715–5730.
[80] L. Escomel, I. Del Rosal, L. Maron, E. Jeanneau, L. Veyre, C. Thieuleux, C. Camp, *J. Am. Chem. Soc.* **2021**, *143*, 4844–4856.
[81] V. Mougel, C. Copéret, *ACS Catal.* **2015**, *5*, 6436–6439.
[82] R. Srivastava, E. A. Quadrelli, C. Camp, *Dalton Trans.* **2020**, *49*, 3120–3128.
[83] "Deposition number 2116170 (for 2) contain the supplementary crystallographic data for this paper. These data are provided free of charge by the joint Cambridge Crystallographic Data Centre and Fachinformationszentrum Karlsruhe Access Structures service.," can be found under https://www.ccdc.cam.ac.uk/structures/? **n.d**.
[84] G. Tosin, C. C. Santini, M. Taoufik, A. De Mallmann, J. M. Basset, *Organometallics* **2006**, *25*, 3324–3335.
[85] G. Tosin, C. C. Santini, A. Baudouin, A. De Mallman, S. Fiddy, C. Dablemont, J. M. Basset, *Organometallics* **2007**, *26*, 4118–4127.
[86] K. M. Altus, J. A. Love, *Commun. Chem.* **2021**, *4*, 1–11.
[87] R. Waterman, *Organometallics* **2013**, *32*, 7249–7263.
[88] C. Thieuleux, A. Maraval, L. Veyre, C. Copéret, D. Soulivong, J.-M. Basset, G. J. Sunley, *Angew. Chem. Int. Ed.* **2007**, *46*, 2288–2290.
[89] J. J. Mortensen, M. Parrinello, *J. Phys. Chem. B* **2000**, *104*, 2901–2907.
[90] X. Zhang, Y. Lu, L. Kovarik, P. Dasari, D. Nagaki, A. M. Karim, *J. Catal.* **2021**, *394*, 376–386.
[91] J. R. Engstrom, D. W. Goodman, W. H. Weinberg, *J. Am. Chem. Soc.* **1988**, *110*, 8305–8319.
[92] J. R. Engstrom, D. W. Goodman, W. H. Weinberg, *J. Am. Chem. Soc.* **1986**, *108*, 4653–4655.
[93] D. W. Flaherty, D. D. Hibbitts, E. Iglesia, *J. Am. Chem. Soc.* **2014**, *136*, 9664–9676.
[94] S. Kawi, J. R. Chang, B. C. Gates, *J. Phys. Chem.* **1994**, *98*, 12978–12988.
[95] S. P. Brown, I. Schnell, J. D. Brand, K. Müllen, H. W. Spiess, *J. Am. Chem. Soc.* **1999**, *121*, 6712–6718.
[96] M. Hohwy, H. J. Jakobsen, M. Edén, M. H. Levitt, N. C. Nielsen, *J. Chem. Phys.* **1998**, *108*, 2686–2694.
[97] D. Marion, M. Ikura, R. Tschudin, A. Bax, *J. Magn. Reson.* **1989**, *85*, 393–399.
[98] M. Carravetta, J. Schmedt auf der Günne, M. H. Levitt, *J. Magn. Reson.* **2003**, *162*, 443–453.
[99] M. Edén, M. H. Levitt, *Chem. Phys. Lett.* **1998**, *293*, 173–179.
[100] I. Schnell, A. Lupulescu, S. Hafner, D. E. Demco, H. W. Spiess, *J. Magn. Reson.* **1998**, *133*, 61–69.
[101] I. Schnell, W. H. Spiess, *J. Magn. Reson.* **2001**, *151*, 153–227.
[102] D. F. Shantz, J. Schmedt Auf Der Günne, H. Koller, R. F. Lobo, *J. Am. Chem. Soc.* **2000**, *122*, 6659–6663.
[103] R. C. Clark, J. S. Reid, *Acta Crystallogr. Sect. A* **1995**, *51*, 887–897.
[104] A. Altomare, M. C. Burla, M. Camalli, G. L. Cascarano, C. Giacovazzo, A. Guagliardi, A. G. G. Moliterni, G. Polidori, R. Spagna, *J. Appl. Crystallogr.* **1999**, *32*, 115–119.
[105] P. W. Betteridge, J. R. Carruthers, R. I. Cooper, K. Prout, D. J. Watkin, *J. Appl. Crystallogr.* **2003**, *36*, 1487–1487.
[106] F. G. Gault, C. Kemball, *Trans. Faraday Soc.* **1961**, *57*, 1781–1794.
[107] T. M. Gilbert, F. J. Hollander, R. G. Bergman, *J. Am. Chem. Soc.* **1985**, *107*, 3508–3516.
[108] P. J. Davidson, M. F. Lappert, R. Pearce, *J. Organomet. Chem.* **1973**, *57*, 269–277.
[109] R. J. P. Corriu, Y. Guari, A. Mehdi, C. Reyé, C. Thieuleux, L. Datas, *Chem. Commun.* **2001**, *37*, 763–764.
[110] C. Coperet, A. Comas-Vives, M. P. Conley, D. P. Estes, A. Fedorov, V. Mougel, H. Nagae, F. Núñez-Zarur, P. A. Zhizhko, C. Copéret, A. Comas-Vives, M. P. Conley, D. P. Estes, A. Fedorov, V. Mougel, H. Nagae, F. Núñez-Zarur, P. A. Zhizhko, *Chem. Rev.* **2016**, *116*, 323–421.
[111] B. Ravel, M. Newville, *J. Synchrotron Radiat.* **2005**, *12*, 537–541.
[112] R. Graf, D. E. Demco, J. Gottwald, S. Hafner, H. W. Spiess, *J. Chem. Phys.* **1997**, *106*, 885–895.
[113] S. P. Brown, H. W. Spiess, *Chem. Rev.* **2001**, *101*, 4125–4155.

Manuscript received: January 15, 2024
Accepted manuscript online: February 19, 2024
Version of record online: ■■, ■■

Research Articles

Heterogeneous Catalysis

A. V. Pichugov, L. Escomel, S. Lassalle, J. Petit, R. Jabbour, D. Gajan, L. Veyre, E. Fonda, A. Lesage, C. Thieuleux, C. Camp* _____ **e202400992**

Highly Selective and Efficient Perdeuteration of n-Pentane via H/D Exchange Catalyzed by a Silica-Supported Hafnium-Iridium Bimetallic Complex

selective perdeuteration

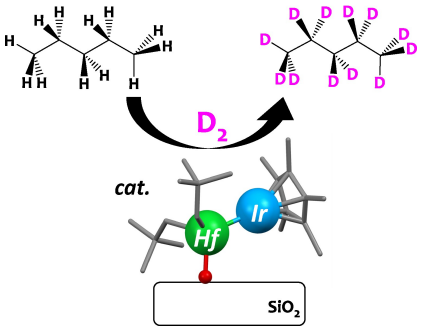

A novel hafnium-iridium complex immobilized on silica, **HfIr/SiO$_2$**, is highly efficient and selective for the perdeuteration of alkanes with D_2, exemplified on *n*-pentane, without substantial deuterogenolysis. This represents substantial advance in catalytic H/D isotope exchange (HIE) reactions of C(sp^3)–H bonds.